Applied Mathematics & Information Sciences
An International Journal

http://dx.doi.org/10.18576/amis/100413

Electronically Coupled Distributed Generation Modeling and Control Strategies for Microgrid Applications

Bilal M. Eid[1,2,*], *Nasrudin Abd. Rahim*[1,3], *Jeyraj Selvaraj*[1] *and B. W. Williams* [4]

[1] UM Power Energy Dedicated Advanced Centre (UMPEDAC) Wisma R & D, University of Malaya 59990 Kuala Lumpur, Malaysia
[2] Department of Electrical Engineering, University of Malaya, 50603 Kuala Lumpur, Malaysia
[3] Renewable Energy Research Group, King Abdulaziz University, 21589 Jeddah, Saudi Arabia
[4] Electronic and Electrical Engineering Department, University of Strathclyde, Glasgow, UK

Received: 26 Mar. 2016, Revised: 12 May 2016, Accepted: 13 May 2016
Published online: 1 Jul. 2016

Abstract: A single-stage power converter is proposed for electronically coupled distributed generation, that is capable of both maximum power point tracking and unity power factor dispatching. Modeling for photovoltaic array (the distributed generator) and three-phase grid-connected inverter produce the optimum control parameters. The inverter's controller uses inner and outer control loops to control parameters. The inner control loop converts input from the abc frame to the d, q, 0 frame to dispatch at unity power factor. The outer voltage control loop tracks the maximum power point through the new technique, which can be used in microgrid applications at the primary control level (local controller). A comparison between produced active power from single-stage and two-stage power converter is illustrated, showing that single-stage has higher efficincy. A comparison is conducted between variable and fixed DC reference voltages in terms of their active power yields for the proposed single-stage converter system. The paper investigates the impact of different ambient disturbances such as varying weather conditions, solar radiation with severe disturbances, and variable PV cell temperature on the active and reactive power yields. The dynamic reference voltage is proposed. Its effectiveness during variable radiations and temperatures are verified by Matlab/Simulink simulations.

Keywords: distributed generation, inverter, photovoltaic, microgrid.

1 Introduction

Distributed renewable energy generation have potential in advanced research that attempts their incorporation into electrical power systems. Their features include zero carbon dioxide emission, low running cost, low maintenance cost, and high abundance; encouraging many governments to pass ambitious policies of up to 20% increase or more of renewable energy resources in power supply resources [31]. Photovoltaic (PV) is one promising renewable energy option, increasingly being integrated into distribution networks. Given that nearly 90% of all grid disturbances occur in the distribution networks [17], the move towards distributed generation integration has had to focus on how to enhance grid reliability and quality within the distribution networks [32]. Despite the advantages of PV resources, there are a few challenges that hinder their widespread exploitation. Power source intermittence is one complex challenge afflicting integration. As for grid-connected PV systems, removing battery backup reduces costs and increases efficiency, but increases the challenge of solar radiation intermittence. The controller must have the ability to overcome input and output power disturbances that arise when a PV distributed source is connected to the public grid [2,12,32].

A power conversion system is needed to transfer power from the PV direct current (DC) to the public grid alternative current (AC). Power conversion systems can be classified into two types, depending on the number of power processing stages: single-stage [28,9,23,30,10,36], and two-stage power conversion systems [27,6,29,14,25,4,16,15] (the latter being the most common configuration for electronically-coupled distributed generator (DG)) (see Fig. (1)). Two-stage conversion systems have two converters; one on the PV side which extracts maximum power from the PV, the other is a synchronized inverter connected to the public-grid side,

* Corresponding author e-mail: b.garadh@gmail.com

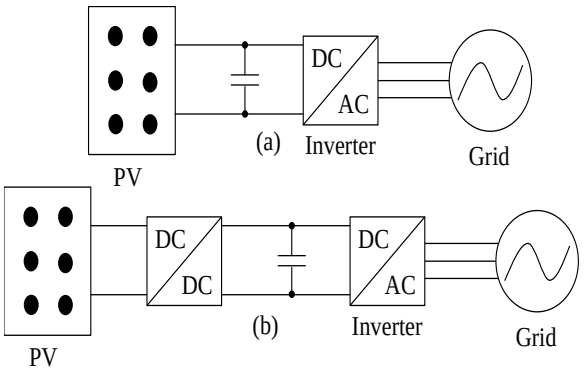

Fig. 1: (a) Single-stage power-conversion system and (b) a two-stage power-conversion system.

which controls the active and reactive power dispatched. In a single-stage approach, the inverter is used alone to meet the power conversion system's requirements. Although Single-stage conversion needs a bulky line transformer, it offers advantages such as high conversion efficiency, simplified topology, low cost, and compactness [38,20,3,10].

As a single stage DC-AC inverter is used as a power converter in this paper, its function is to track the DC link voltage that extracts maximum power from the PV and dispatches zero reactive power to the public grid. The proposed control technique (for voltage source inverters (VSIs)) achieves fast dynamic response through an outer dc link voltage control loop and an inner current control loop. The current control strategy plays the main role in power flow performance. It uses the d, q reference frame which is able to eliminate steady-state error and, through decoupled control has a fast transient response [21]. IEEE standards [1] have been observed, applicable to all distributed resources with aggregate capacity of 10 MVA or less. The following sections of the paper are organized as follows: Section 2 presents the circuit and modeling; Section 3 describes the voltage and current control; Section 4 overviews the control layers of a microgrid; Section 5 presents the simulation results and discussion; then Section 6 concludes the paper.

2 Circuit Description and modeling

Fig. (2) shows a PV energy source connected to a three-phase public grid via a single-stage power conversion system, namely an inverter. The inverter has two loops: an inner loop to control the reactive power and maintain unity power factor, and an outer loop to control reference DC voltage so as to remain at a voltage that extracts maximum power from the PV. The inverter switching technique is pulse width modulation (PWM),the switches operate at constant frequency which is much higher than the line frequency. PWM produces pulses to comply with maximum power point tracking (MPPT), unity power factor mode, and synchronization with the public grid. A filter is used to remove undesired frequency components and enhance the desired ones. The inductors are linear and balanced. The whole conduction losses are represented by three symmetrical resistors. The filter output is connected to the secondary side of a step down transformer (96 winding turns ratio). The transformer's primary is connected to the high voltage public grid. The measurement block at main bus (B), measures the output voltage and current. The controllable part in this system is the inverter. More details about the inner and outer loops are presented in section 3.

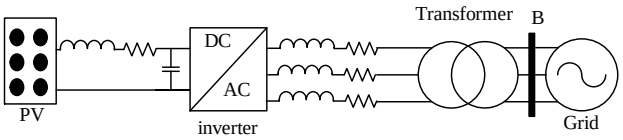

Fig. 2: Photovoltaic arrays connected to the public grid.

2.1 PV modeling

The solar cell is the energy producing part of the PV panel. Fig. (3) shows an equivalent circuit for a solar cell [38,21, 4]. It can be represented by a current source connected in parallel with a diode. The output current I_o is given by:

$$I_o = I_{ph} - I_d - \frac{V_d}{R_{sh}} \quad (1)$$

I_{ph} is the photocurrent V_d is the diode voltage, R_{sh} is the equivalent shunt resistance and I_d is the diode current which equals:

$$I_d = I_{rsc} * ((\exp \frac{q.V_d}{\eta.k.T}) - 1) \quad (2)$$

I_{rsc} is the diode reverse saturation current, q is the electron charge 1.6* 10^{-19} C , k is Boltzman's constant 1.38 * 10^{-23} J/K , η is the diode quality factor, T is the PV panel temperature. The output voltage V_o is given by:

$$V_o = V_d - I_o R_s \quad (3)$$

where R_s is the series resistance. In general, the output current I_o of the solar cell is:

$$I_o = I_{ph} - I_{rsc} * ((\exp \frac{q.(V_o + I_o R_s)}{\eta.k.T}) - 1) - \frac{(V_o + I_o R_s)}{R_{sh}} \quad (4)$$

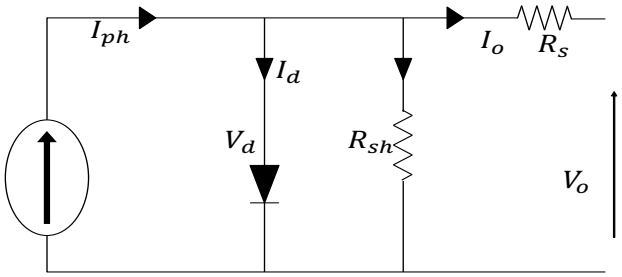

Fig. 3: Photovoltaic cell equivalent circuit.

R_s is usually low and R_{sh} high; so they can be neglected. Equation (4) can be simplified to:

$$I_o = I_{ph} - I_{rsc} * ((\exp \frac{q.V_o}{\eta.k.T}) - 1) \quad (5)$$

During open circuit, the output current I_o equals zero. Furthermore, the shunt resistance is considered to be very large, so the open-circuit V_{oc} from (5) is:

$$V_{oc} = (\frac{\eta.T.k}{q}) \ln(\frac{I_{ph}}{I_{rsc}} + 1) \quad (6)$$

During short circuit, the output voltage V_o equals zero and I_{rsc} can be neglected so the output short-circuit current I_{sc} from (4) is:

$$I_{sc} = \frac{I_{ph}}{(1 + \frac{R_s}{R_{sh}})} \quad (7)$$

The output power equation is:

$$P = V_o I_o = V_o(I_{ph} - I_d - \frac{V_d}{R_{sh}}) \quad (8)$$

The solar radiation I is:

$$I = \phi * E \quad (9)$$

where ϕ is the photon flux, which represents the number of photons per unit time per unit area. E is photon energy, obtainable from:

$$E = \frac{hc}{\lambda} \quad (10)$$

where h is Planck's constant $6.626*10^{-34}$ j.s , c is the light speed in a vacuum $3*10^8$ m/s . λ the wavelength.

2.2 Nominal operating cell temperature (Malaysia)

The cell temperature (T_c) plays the main role in assessing the efficiency of a solar cell. The value of T_c is calculated based on ambient temperature and solar radiation values as well as the nominal operating cell temperature (NOCT). NOCT is defined as the temperature element in a solar cell exposed at 800 W/m^2 of solar radiation, 20°C of ambient temperature, and a wind speed of 1 m/s. As these conditions may vary depending on the climate zone nature, the paper [37] proposed a new condition called tropical field operation cell temperature (tFOCT) suitable for tropical zones like Malaysia. The results show that the suitable weather conditions for measuring the tFOCT are 886 W/m^2 of solar radiation, 34°C of ambient temperature, and a wind speed of 3.2 m/s, Concluding that the recommended tFOCT value is 52.5°C. Therefore the T_c can be obtained by below equation:

$$T_c = T_a + G * \frac{(tFOCT - 34°C)}{886 W/m^2} \quad (11)$$

where T_c and T_a are the cell and the ambient temperatures respectively, G is the instant solar radiation.

The experimental tests for the PV panels reveal that the efficiency decreases with the T_c increases. From (1) and (2) the output current I_o increases slightly with the temperature, while temperature affects various other terms in (6), net effect of temperature is that it decreases V_{oc} linearly. The drop in V_{oc} with temperature is mainly related to the increase in the diode reverse saturation current I_{rsc} which strongly depends on the temperature. The common rule for I_{rsc} and T_c relation is that I_{rsc} doubles for every 10°C rise in T_c [8]. Therefore, the relation between diode saturation current and temperature can be expressed by the (12)

$$I_{rsc} = I_{rsc,STC} * 2^{(\frac{T_c - 298°}{10})} \quad (12)$$

where $I_{rsc,STC}$ is the diode saturation current at the standard test condition.

2.3 VSI modeling

The three-phase VSI connected to a grid is shown in Fig. (4). To achieve VSI modeling, the assumption of symmetrical and sinusoidal three phase voltage is adopted as shown in (13):

$$\left\{ \begin{array}{c} v_a = V_m cos(wt) \\ v_b = V_m cos(wt - \frac{2}{3}\pi) \\ v_c = V_m cos(wt + \frac{2}{3}\pi) \end{array} \right\} \quad (13)$$

Where V_m is the peak value of the voltage, so the VSI model in the abc frame is:

$$\left\{ \begin{array}{c} e_a = L\frac{di_a}{dt} + i_a R + v_a + v_{nN} \\ e_b = L\frac{di_b}{dt} + i_b R + v_b + v_{nN} \\ e_c = L\frac{di_c}{dt} + i_c R + v_c + v_{nN} \\ I_{pv} = C\frac{dv_{dc}}{dt} + i_{inv} \end{array} \right\} \quad (14)$$

R and C are the resistor and capacitors respectively shown in Fig. (4), from (14)

$$v_{nN} = \frac{1}{3}(e_a + e_b + e_c) \quad (15)$$

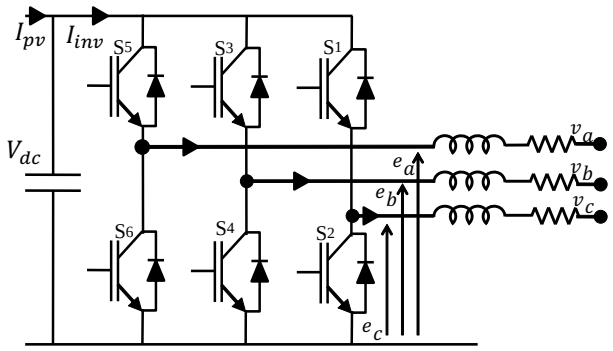

Fig. 4: Three-phase voltage source inverter.

The inverter's switching function $d_k^*(k=1,3,5)$ is defined as

$$d_k^* = \begin{Bmatrix} 1, & if\ S_k\ is\ on\ and\ S_{k+1}\ is\ off \\ 0, & if\ S_k\ is\ off\ and\ S_{k+1}\ is\ on \end{Bmatrix} \quad (16)$$

The voltage values per phase are calculated based on switch position at that period from the Equ below:

$$e_a - VnN = V_{dc}(d_1^* - \frac{d_1^*+d_3^*+d_5^*}{3}) \quad (17)$$

Therefore, the model can be written as in Equation (18)

$$\begin{Bmatrix} L\frac{di_a}{dt} = -i_aR - v_a + (d_1^* - \frac{d_1^*+d_3^*+d_5^*}{3})v_{dc} \\ L\frac{di_b}{dt} = -i_bR - v_b + (d_3^* - \frac{d_1^*+d_3^*+d_5^*}{3})v_{dc} \\ L\frac{di_c}{dt} = -i_aR - v_c + (d_5^* - \frac{d_1^*+d_3^*+d_5^*}{3})v_{dc} \\ C\frac{dv_{dc}}{dt} = I_{pv} - (d_1^*i_a + d_3^*i_b + d_5^*i_c) \end{Bmatrix} \quad (18)$$

For PWM inputs Equ. (18) can be separated into high-frequency and low-frequency components following Fourier analysis. The low-frequency component is the same as Equ. (18), with the switching functions d^* being replaced by continuous duty ratios $d_k^*(k=1,3,5)$, containing $\in [0,1]$ is considered further in [35]

$$T_{dq0}^{abc} = \frac{2}{3}\begin{bmatrix} cos(wt) & cos(wt-\frac{2}{3}\pi) & cos(wt+\frac{2}{3}\pi) \\ sin(wt) & sin(wt-\frac{2}{3}\pi) & sin(wt+\frac{2}{3}\pi) \\ \frac{1}{2} & \frac{1}{2} & \frac{1}{2} \end{bmatrix} \quad (19)$$

The model described by Equ (18) are time varying and nonlinear. Control can be facilitated by transforming the model into a synchronous orthogonal frame rotating at the utility angular frequency ω. The positive-sequence components at the fundamental frequency become constant and the resultant time-varying transformation is given by Equ (19). From Eqs (18) and (19) an expression in dq frame for the whole dynamic model is:

$$\begin{bmatrix} \frac{di_d}{dt} \\ \frac{di_q}{dt} \\ \frac{dv_{dc}}{dt} \end{bmatrix} = \begin{bmatrix} -\frac{R}{L} & \omega & \frac{d_d}{L} \\ -\omega & -\frac{R}{L} & \frac{d_q}{L} \\ -\frac{d_d}{C} & -\frac{d_q}{C} & 0 \end{bmatrix} \begin{bmatrix} i_d \\ i_q \\ v_{dc} \end{bmatrix} + \begin{bmatrix} -\frac{1}{L} & 0 & 0 \\ 0 & -\frac{1}{L} & 0 \\ 0 & 0 & \frac{1}{C} \end{bmatrix} \begin{bmatrix} v_d \\ v_q \\ I_{pv} \end{bmatrix} \quad (20)$$

where:
i_d is d axis grid currents;
i_q is q axis grid currents;
v_d is d axis grid voltages;
v_q is q axis grid voltages;
d_d is d axis duty ratios;
d_q is q axis duty ratios;

3 System controllers

3.1 Outer loop controller

Model (20) shows the third equation representing voltage control. At unity power factor (i_q=0), this equation can be simplified to:

$$C\frac{dV_{dc}}{d_t} = I_{pv} - i_d d_d \quad (21)$$

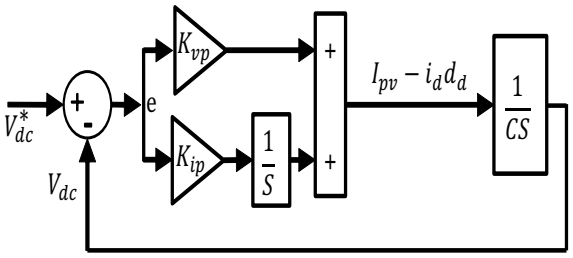

Fig. 5: Voltage loop control.

The error $e = V_{dc}^* - V_{dc}$ passes through a PI-type regulator as depicted in Fig. (5) to regulate the dc voltage to a fixed value. The controller used to balance the power between the DC-link and the public grid as well as to determine the amount of current injected into or absorbed by the public grid [5].In Figs. (5) and (6), the voltage loop is an outer loop whereas the current loop is an inner loop. The internal loop can be designed to achieve a short settling time and fast error correction. Thus, the outer and inner loops can be considered decoupled and can be linearized. The closed-loop transfer function of the dc voltage regulation, obtained from Fig. (5), can be expressed in the following form:

$$\frac{V_{dc}(s)}{V_{dc}^*(s)} = \frac{k_{vp}}{C}\frac{\frac{k_{vi}}{k_{vp}}+S}{S^2+\frac{k_{vp}}{C}S+\frac{k_{vi}}{C}} \quad (22)$$

The damping ratio is $\zeta = (k_{vp})/2C\sqrt{k_{vi}/C}$, and $\omega_{nv}^2 = k_{vi}/C$. Thus the voltage regulator parameters are:

$$\begin{matrix} k_{vp} = 2\zeta C\omega_{nv} \\ k_{vi} = C\omega_{nv}^2 \end{matrix} \quad (23)$$

3.2 Inner loop controller

Model expressed by (20) shows that there is a cross-coupling between the d and q components, which affects the dynamic performance of the regulator [21]. Therefore, for better performance, decoupling the two axes is necessary, which can be accomplished by feedforward decoupling control method. Assuming:

$$\left.\begin{array}{l} v_{rd} = -V_d + d_d V_{dc} + \omega L i_q \\ v_{rq} = -V_q + d_q V_{dc} + \omega L i_d \end{array}\right\} \quad (24)$$

Then from the model given by (20), the system expressions become

$$\left\{\begin{array}{c} \frac{di_d}{dt} = -\frac{R}{L} i_d + \frac{1}{L} v_{rd} \\ \frac{di_q}{dt} = -\frac{R}{L} i_q + \frac{1}{L} v_{rq} \\ \frac{dv_{dc}}{dt} = \frac{I_{pv}}{C} - \frac{V_d + v_{rd}}{CV_{dc}} i_d - \frac{V_q + v_{rq}}{CV_{dc}} i_q \end{array}\right\} \quad (25)$$

Model (25) eliminates the cross-coupling variables. Therefore, the currents i_d and i_q can be controlled independently by acting upon inputs V_d and V_q, respectively. Moreover, by using a PI-type compensation, zero steady-state error and a fast dynamic response can be achieved. The current regulator diagram is shown in Fig. (6). The sampling and hold delay can be neglected, since the line frequency is much less than the switching frequency. In Fig. (6), k_{ip} and k_{ii} are respectively the proportional and integral parameters, i^* and i respectively are the reference current signal and feedback current. The figure is suitable for both the i_d and i_q loops. From the figure, the closed-loop transfer function of the dq current loops is:

$$\frac{i_q(s)}{i_q^*(s)} = \frac{i_d(s)}{i_d^*(s)} = \frac{k_{ip}}{L} \frac{\frac{k_{ii}}{k_{ip}} + S}{S^2 + \frac{k_{ip}+R}{L} S + \frac{k_{ii}}{L}} \quad (26)$$

The damping ratio is $\zeta = (k_{ip} + R)/2L\sqrt{k_{ii}/L}$, and $\omega_{ni}^2 = k_{ii}/L$. Thus the current control parameters are:

$$\begin{array}{c} k_{ip} = 2\zeta\omega_{ni} L - R \\ k_{ii} = L\omega_{ni}^2 \end{array} \quad (27)$$

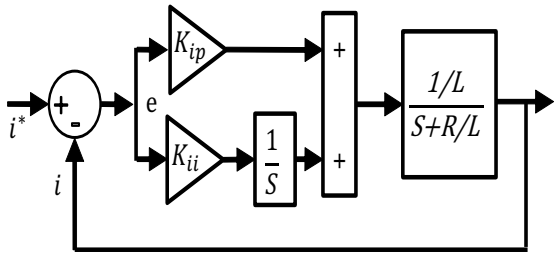

Fig. 6: Current loop control with constant irradiation.

4 Control layers in the Microgrid

The microgrid control system has to ensure that all the control functions are accomplished (e.g., supply of electrical and/or thermal energy, continuous feeding of critical loads, energy-market participation, auto-reconnection after failure, etc.). The control objectives can be achieved through either centralized or decentralized control, and through three control layers as shown in Fig. (7). Some [26,11] call the supervisory control architecture a multi-agent controller. The control levels are [9,26,22,7,33,18,19]:

–Distribution Network Operator (DNO) and Market Operator (MO);
–Microgrid Central Controller (MGCC); and
–Local Controller (LC); which can be either a Source Controller or a Micro Load Controller.

DNO is necessary where there is more than one microgrid in the distribution system. Also, for the market environment of a specific area, one MO or more is responsible for market management of the microgrid. Both DNO and MO are part of the main grid; they do not belong to the microgrid. The second level is the MGCC, which is the main integrator of the DG clusters in a microgrid. It is responsible in stabilizing the voltage and frequency at the point of common coupling (PCC), and responsible for the active and reactive powers dispatched from each DG [7,34] . The LCs are the lower layer of control (sometimes called peer to peer [26]). As shown in this paper, LCs control the DERs and some of the local loads, and seek to balance active and reactive powers. They have a certain intelligence level, thus can make decisions locally in a decentralized operation model (whereas in a centralized model they receive set points from the MGCC) [22,24]. Fig. (7) shows the DNO, MGCC, and LC control layers.

5 Simulations: Results and Discussions

The outer voltage control loop regulates the DC link voltage to extract maximum power from the PV (Fig. (8)). DC-measured voltage ($V_{dc,mes}$), DC-measured current ($I_{dc,mes}$) are the inputs of the MPPT, which continuously compares the present and past values of power, voltage, and current, then appropriately increases or decreases the reference voltage (V_{ref}). Proportional and integral (PI) controllers are used, producing the output $I_{d,ref}$, which feeds the inner loop controller input.

Fig. (9) shows the inner loop controller function using Matlab/Simulink, which controls the reactive power dispatched to the utility, in this study $I_{q,ref}$ is set to zero to maintain unity power factor. $V_{abc,B}$ and $I_{abc,B}$ are the three-phase voltage and current measured at bus bar B (Fig (2)). The phase locked loop (PLL) block converts them from the three-phase reference frame to dq0

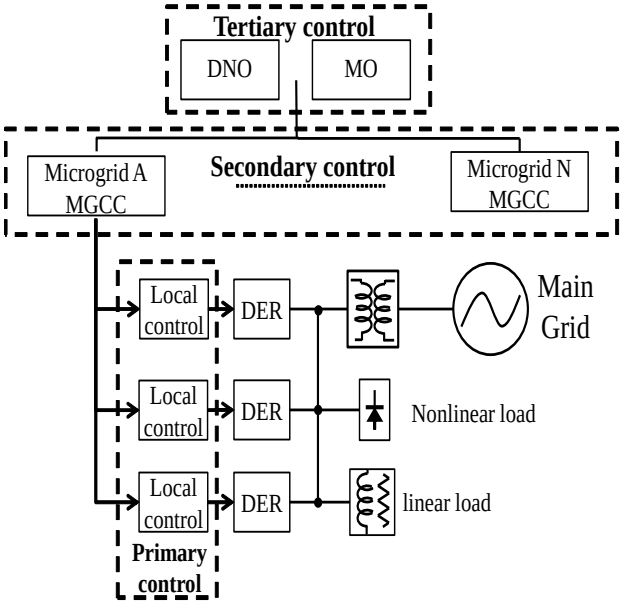

Fig. 7: General architecture of hierarchical microgrid control system.

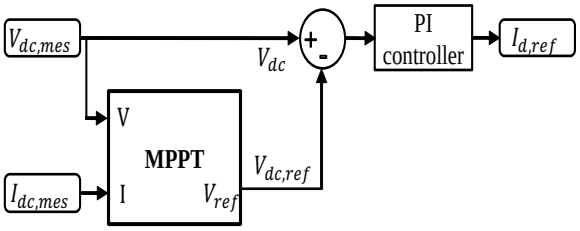

Fig. 8: DC voltage regulator.

reference frame. The values are then used by the reactive power regulator to give the Vd, Vq that operate the system in a unity power factor mode. These signals are used by the PWM generator to produce the desired switch pulses. The control systems use a sample time of 100 μs in the voltage and current controllers and also the PLL synchronization unit. However, the sampling time for the power system is shorter; taking 10μ s to make the simulation run faster. The value of $I_{d,ref}$ comes from the outer loop.

The system runs for 5 s in all the cases to follow. The radiation was changed during this time as shown in Table (1). SunPower SPR-305-WHT PV panels were used. The number of series-connected modules per string is 5, while the number of parallel strings is 66. At 1000 W/m^2 the panels provide 100 kW , with the open circuit voltage (V_{oc}), short circuit current (I_{sc}), voltage at maximum power (V_{mp}), and current at maximum power (I_{mp}) being 64.2 V , 5.96 A , 54.7 V , and 5.58 A , respectively.

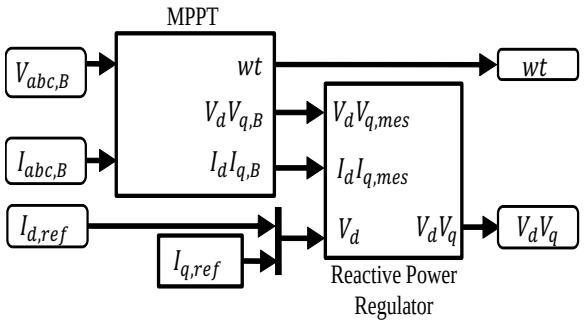

Fig. 9: Reactive power regulator (inner loop).

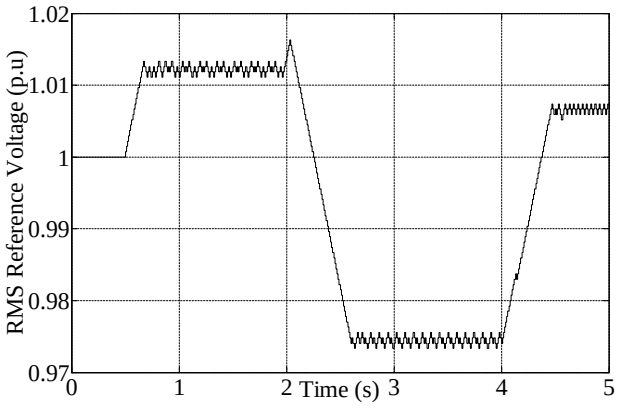

Fig. 10: The voltage reference value.

Parameters of PV module used in this paper are cited in Table (2).

Table 1: The solar radiation on the PV panel

Radiation W/m^2	Time (s)	
	From	To
1000	0	2
700	2	4
900	4	5

5.1 Proposed voltage reference value

5.1.1 Variable radiation

This study proposes a variable voltage reference (V_{ref}) instead of being fixed as in past studies [13]; the reference voltage value changes as in Fig. (10). This technique increases the active power extracted from system, as Fig.

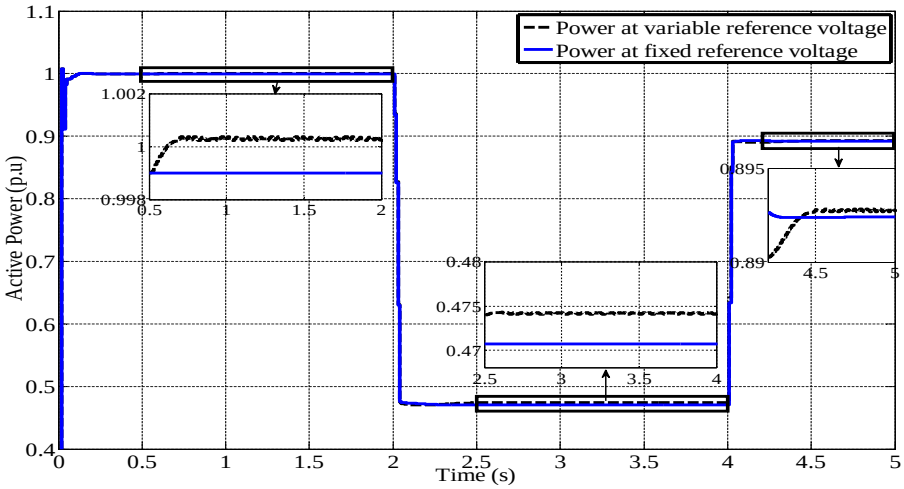

Fig. 11: Active power dispatched to the public grid, with variable and fixed voltage references.

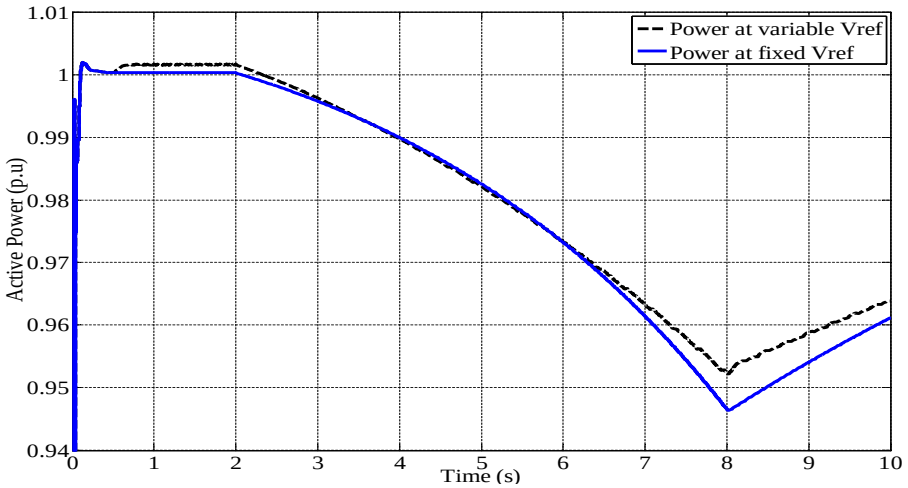

Fig. 12: Active power dispatched to the public grid with variable temperature

Table 2: Electrical specifications of the SunPower PV panels

Parameter	**Value**
Number of cells in series	96
Maximum power (Pmp) [W]	305.2
Maximum power voltage (Vmp) [V]	54.7
Maximum power current (Imp) [A]	5.58
Open circuit voltage (Voc) [V]	64.2
Short circuit current (Isc) [A]	5.96
Series resistance of PV model (Rs) [ohms]	3.80e-02
Parallel resistance of PV model (Rsh) [ohms]	9.94e+02
Diode reverse saturation current (Irsc) [A]	3.19e-08
Light-generated photo-current (Iph) [A]	5.96
Diode quality factor of PV model (η)	1.3

(11) illustrates; the black dashed line (which is the proposed technique) dispatches higher power than the fixed reference (blue continuous) at all solar radiance levels. The correlation between Figs. (10), (11) show that the reference voltage decreased when the radiation dropped aiming to increase the extracted active power at the certain radiation level.

5.1.2 Variable temperature

Fig (12) shows the active power dispatched to the public grid during variable temperature. The cell temperature (T_c) increased from 25° C to 65°C during the first 8 seconds then it decreased gradually. Although, the active power decrease with increasing of the T_c, the proposed technique (dashed black line) achieves higher dispatching active power at steady state compared the continuous blue

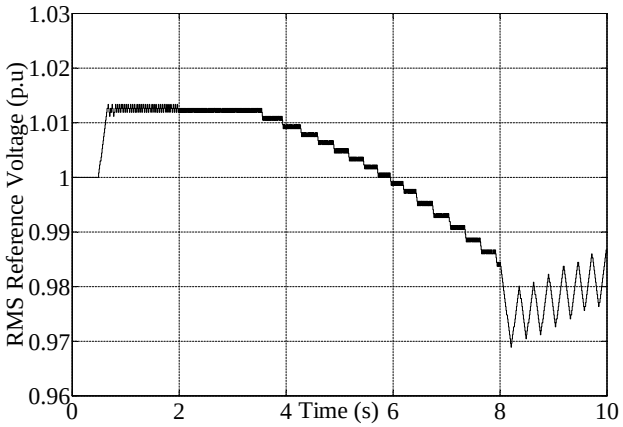

Fig. 13: Reference voltage during variable temperature

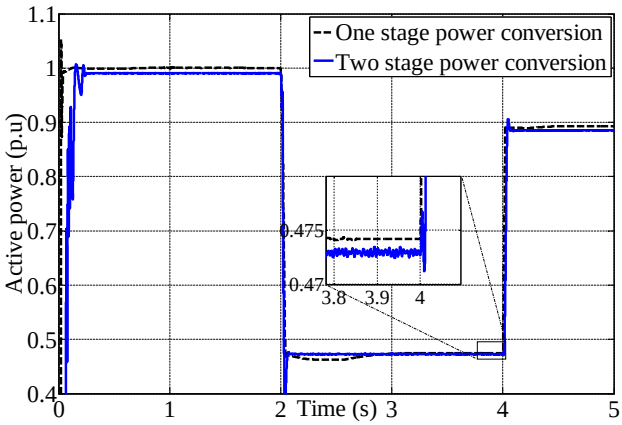

Fig. 14: The active power in single-stage and two-stage power conversion systems.

line (which uses fixed dc voltage reference). Fig (13), illustrates the voltage reference changes with the variable temperature. The correlation between Figs. (13), Fig (12) show that the reference voltage decreased when the temperature increase aiming to increase the extracted active power at the certain temperature level.

5.2 Power flow at single and two stages power conversion

As active power flows from the PV to the utility, losses occur in the conversion system. This paper proposes a single-stage power conversion system, whose efficiency is higher than the two stage power conversion system studied in [13]. Fig. (14) shows the active power exported to the grid with single-stage (dashed line) and two stages (continuous line). The base active power is 100 kW. The power extracted from single-stage is higher for the three solar radiation levels as the Fig. (14) shows, revealing that the efficiency with single-stage power conversion is higher.

5.3 Reactive power

As in some previous works [4], the system dispatches unity power factor, and the reactive power injected into the grid is set to zero. Fig. (15) shows the reactive power dispatched to the public grid during (1) variable solar radiation, and (2) variable temperature. The reactive power disrupts at 2 s and 4 s when the solar radiation changes, but the controller overcomes the disturbance and returns the reactive power back to zero. The base reactive power is 100 kVAr.

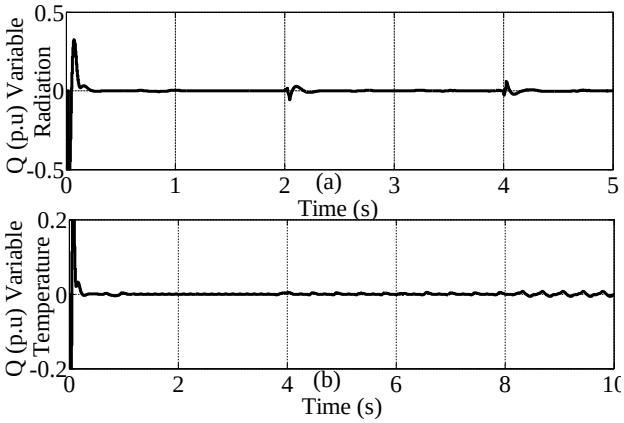

Fig. 15: The reactive power dispatched from the PV system to the grid, (1) with variable solar radiation, (2) with variable cell temperature.

5.4 Voltage and Current

Figs. (16) and (17) show the line-to-ground RMS voltage and current at the PCC. The voltage and the current basis are 14433 V and 3.35 A, respectively. The RMS voltage is constant around 1.4 kV. Fig. (17) shows the current imported to the grid, which is directly proportional to the active power provided by the PV source. Current reaches to the minimum between 2 s to 4 s due to the drop of solar radiation during that period. Fig. (18) shows the sinusoidal voltage and current at the PCC, illustrating that both have low distortion and the phase shift is almost zero, that is unity power factor.

6 Conclusion

In this paper a single-stage power conversion system was studied. An inverter is the only power conversion

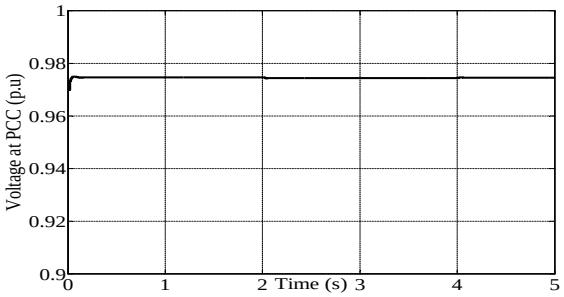

Fig. 16: RMS Voltage at the PCC.

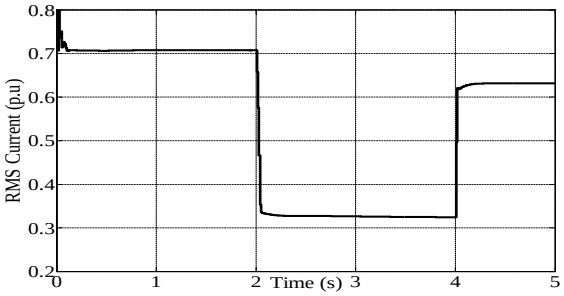

Fig. 17: RMS Current at the PCC.

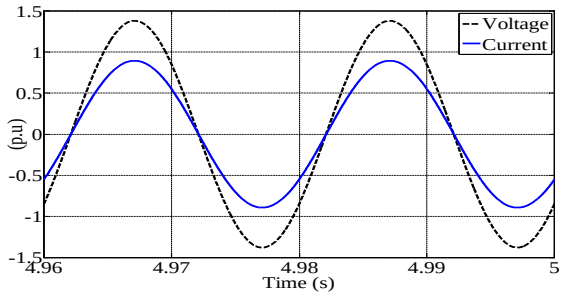

Fig. 18: The voltage and current sine waves.

component used. It achieved two tasks: maximum power point tracking (MPPT) and unity power factor dispatching to the public grid. The study revealed that the dispatched active power is higher than a two-stage power conversion system. A variable reference voltage was used to extract the maximum power from the system. This technique can extract higher active power from PV panel during variable solar radiation and cell temperature. Unity power factor operation shows that the single-stage power conversion system performs all tasks properly.

Acknowledgement

The authors thank the technical and financial assistance of the UM Power Energy Dedicated Advanced (UMPEDAC) and the High Impact Research Grant, Campus Network Smart Grid for Energy Security (H-16001-00-D000032). The authors are grateful to the anonymous referee for a careful checking of the details and for helpful comments that improved this paper.

References

[1] Ieee standard for interconnecting distributed resources with electric power systems. *IEEE Std 1547-2003*, 2003.

[2] P. F. Acuna, L. A. Morn, C. A. Weishaupt, and J. W. Dixon. An active power filter implemented with multilevel single-phase npc converters. In *IECON 2011-37th Annual Conference on IEEE Industrial Electronics Society*, pages 4367–4372. IEEE.

[3] B. Alajmi, K. Ahmed, G. Adam, and B. Williams. Single-phase single-stage transformer less grid-connected pv system. *Power Electronics, IEEE Transactions on*, 28(6):2664–2676, June 2013.

[4] S. Balathandayuthapani, C. Edrington, S. Henry, and J. Cao. Analysis and control of a photovoltaic system: Application to a high-penetration case study. *Systems Journal, IEEE*, 6(2):213–219, June 2012.

[5] R. Bastos, C. Aguiar, A. Goncalves, and R. Machado. An intelligent control system used to improve energy production from alternative sources with dc/dc integration. *Smart Grid, IEEE Transactions on*, 5(5):2486–2495, Sept 2014.

[6] F. Blaabjerg, Z. Chen, and S. Kjaer. Power electronics as efficient interface in dispersed power generation systems. *Power Electronics, IEEE Transactions on*, 19(5), 2004.

[7] Z. Bo, Z. Xuesong, and C. Jian. Integrated microgrid laboratory system. *Power Systems, IEEE Transactions on*, 27(4), 2012.

[8] T. F. Bogart Jr. Electronic devices and circuits, 1986.

[9] Z. Chen. A review of power electronics based microgrids. *Journal of Power Electronics*, 12(1), 2012.

[10] M. Das and V. Agarwal. Novel pv fed three phase single power stage system for stand-alone applications. In *Photovoltaic Specialists Conference (PVSC), 2012 38th IEEE*, pages 001405–001410. IEEE, 2012.

[11] A. L. Dimeas and N. D. Hatziargyriou. Operation of a multiagent system for microgrid control. *Power Systems, IEEE Transactions on*, 20(3), 2005.

[12] J. Dixon, L. Moran, J. Rodriguez, and R. Domke. Reactive power compensation technologies: state-of-the-art review. *Proceedings of the IEEE*, 93(12), 2005.

[13] B. Eid, N. Rahim, and J. Selvaraj. Distributed photovoltaic generator performing reactive power compensation. In *Clean Energy and Technology (CEAT), 2013 IEEE Conference on*, pages 38–41, Nov 2013.

[14] B. Eid, N. Rahim, J. Selvaraj, and A. El Khateb. Control methods and objectives for electronically coupled distributed energy resources in microgrids: A review. *Systems Journal, IEEE*, PP(99):1–13, 2014.

[15] A. El Khateb, N. Rahim, J. Selvaraj, and M. Uddin. Fuzzy logic controller based sepic converter for maximum power point tracking. *Industry Applications, IEEE Transactions on*, PP(99):1–1, 2014.

[16] A. El Khateb, N. A. Rahim, J. Selvaraj, and M. N. Uddin. Maximum power point tracking of single-ended primary-inductor converter employing a novel optimisation technique for proportional-integral-derivative controller. *IET Power Electronics*, 6(6), 2013.

[17] H. Farhangi. The path of the smart grid. *Power and Energy Magazine, IEEE*, 8(1):18–28, January 2010.

[18] J. Guerrero, J. Vasquez, J. Matas, M. Castilla, and L. de Vicuna. Control strategy for flexible microgrid based on parallel line-interactive ups systems. *Industrial Electronics, IEEE Transactions on*, 56(3), 2009.

[19] J. Guerrero, J. Vasquez, J. Matas, L. de Vicua, and M. Castilla. Hierarchical control of droop-controlled ac and dc microgridsa general approach toward standardization. *Industrial Electronics, IEEE Transactions on*, 58(1), 2011.

[20] M. Jang and V. Agelidis. A minimum power-processing-stage fuel-cell energy system based on a boost-inverter with a bidirectional backup battery storage. *Power Electronics, IEEE Transactions on*, 26(5):1568–1577, May 2011.

[21] R. Kadri, J.-P. Gaubert, and G. Champenois. An improved maximum power point tracking for photovoltaic grid-connected inverter based on voltage-oriented control. *Industrial Electronics, IEEE Transactions on*, 58(1):66–75, 2011.

[22] F. Katiraei, R. Iravani, N. Hatziargyriou, and A. Dimeas. Microgrids management. *Power and Energy Magazine, IEEE*, 6(3), 2008.

[23] S. Kjaer, J. Pedersen, and F. Blaabjerg. A review of single-phase grid-connected inverters for photovoltaic modules. *Industry Applications, IEEE Transactions on*, 41(5), 2005.

[24] R. Lasseter and P. Piagi. Control and design of microgrid components. *PSERC Publication 06*, 3, 2006.

[25] Y. Liu, J. Bebic, B. Kroposki, J. de Bedout, and W. Ren. Distribution system voltage performance analysis for high-penetration pv. In *Energy 2030 Conference, 2008. ENERGY 2008. IEEE*, pages 1–8. IEEE.

[26] M. Mao, C. Liuchen, and M. Ding. Integration and intelligent control of micro-grids with multi-energy generations: A review. In *Sustainable Energy Technologies, 2008. ICSET 2008. IEEE International Conference on*, pages 777–780, 2008.

[27] S. Munir and Y. W. Li. Residential distribution system harmonic compensation using pv interfacing inverter. *Smart Grid, IEEE Transactions on*, 4(2):816–827, 2013.

[28] S. Ozdemir, N. Altin, and I. Sefa. Single stage three level grid interactive {MPPT} inverter for {PV} systems. *Energy Conversion and Management*, 80(0):561 – 572, 2014.

[29] S. Ponnaluri, G. Linhofer, J. Steinke, and P. Steimer. Comparison of single and two stage topologies for interface of bess or fuel cell system using the abb standard power electronics building blocks. In *Power Electronics and Applications, 2005 European Conference on*, pages 9 pp.–P. 9. IEEE, 2005.

[30] N. A. Rahim and A. M. Omar. Three-phase single-stage high-voltage dc converter. *Generation, Transmission and Distribution, IEE Proceedings-*, 149(5), 2002.

[31] T. Schenk and L. Stokes. The power of collaboration: Engaging all parties in renewable energy infrastructure development. *Power and Energy Magazine, IEEE*, 11(3):56–65, May 2013.

[32] A. K. Srivastava, A. A. Kumar, and N. N. Schulz. Impact of distributed generations with energy storage devices on the electric grid. *Systems Journal, IEEE*, 6(1), 2012.

[33] A. Tuladhar, H. Jin, T. Unger, and K. Mauch. Control of parallel inverters in distributed ac power systems with consideration of line impedance effect. *Industry Applications, IEEE Transactions on*, 36(1), 2000.

[34] T. S. Ustun, C. Ozansoy, and A. Zayegh. Recent developments in microgrids and example cases around the worlda review. *Renewable and Sustainable Energy Reviews*, 15(8), 2011.

[35] R. Wu, S. B. Dewan, and G. R. Slemon. Analysis of an ac-to-dc voltage source converter using pwm with phase and amplitude control. *Industry Applications, IEEE Transactions on*, 27(2):355–364, 1991.

[36] W. Xiao, F. F. Edwin, G. Spagnuolo, and J. Jatskevich. Efficient approaches for modeling and simulating photovoltaic power systems. *Photovoltaics, IEEE Journal of*, 3(1):500–508, 2013.

[37] M. E. Ya'acob, H. Hizam, T. Khatib, M. A. M. Radzi, C. Gomes, M. H. Marhaban, W. Elmenreich, et al. Modelling of photovoltaic array temperature in a tropical site using generalized extreme value distribution. *Journal of Renewable and Sustainable Energy*, 6(3):033134, 2014.

[38] A. Yazdani, A. Di Fazio, H. Ghoddami, M. Russo, M. Kazerani, J. Jatskevich, K. Strunz, S. Leva, and J. Martinez. Modeling guidelines and a benchmark for power system simulation studies of three-phase single-stage photovoltaic systems. *Power Delivery, IEEE Transactions on*, 26(2):1247–1264, April 2011.

Bilal Eid received the B.Sc from the faculty of engineering, Sana'a University, Yemen, in 2008. The M. Sc. degree in electrical energy and power systems from University of Malaya, Malaysia, in 2011. Currently, PhD candidate in the field of Microgrids and renewable energy integration at faculty of engineering University of Malaya. Since 2011 till now, he is a research assistant with power energy dedicated advanced centre (UMPEDAC), University of Malaya. His main research interests include; Microgrid, smart grids, power conversion systems, renewable energy, photovoltaic inverters and dc-dc converters.

Nasrudin Abd Rahim received the B.Sc. (Hons.) and M.Sc. degrees from the University of Strathclyde, Glasgow, U.K., in 1985 and 1988, respectively, and the Ph.D. degree from Heriot-Watt University, Edinburgh, U.K., in 1995. Currently, he is a Professor with the University of Malaya, where he is the Director of power energy dedicated advanced centre (UMPEDAC) and the Chairman of the University of Malaya Advanced Engineering and Technology Research Cluster. His research interests include power electronics, real-time control systems, electrical drives, and renewable energy systems. Prof. Nasrudin is a Fellow of the Academy of Sciences Malaysia and the Institution of Engineering and Technology, U.K., and is a Chartered Engineer.

Jeyraj Selvaraj received the B.Eng.(Hons.) degree from Multimedia University, Cyberjaya, Malaysia, in 2002, the M.Sc. degree in power electronics and drives jointly from the University of Birmingham, Birmingham, U.K., and the University of Nottingham, Nottingham, U.K., in 2004, and the Ph.D. degree from the University of Malaya, Kuala Lumpur, Malaysia, in 2009. He is currently with power energy dedicated advanced centre (UMPEDAC), University of Malaya. His research interests are single- and three-phase multilevel inverters, digital current-control techniques, photovoltaic inverters, and dc-dc converters.

Barry W. Williams received the M.Eng.Sc. degree from the University of Adelaide, Adelaide, Australia, in 1978, and the Ph.D. degree from Cambridge University, Cambridge, U.K., in 1980. For seven years, he was a Lecturer at Imperial College, University of London, London, U.K. In 1986, he was appointed as the Chair of Electrical Engineering at Heriot-Watt University, Edinburgh, U.K. Currently, he is a Professor at the University of Strathclyde, Glasgow, U.K., where he is engaged in power electronics (in which he has a free Internet text) and drive systems research. His current research interests include power semiconductor modeling and protection, converter topologies, soft-switching techniques, and application of application-specified integrated circuits and DSPs to industrial electronics and renewable energy.